ELSEVIER

Sensors and Actuators 2839 (2000) 1–11

SENSORS AND ACTUATORS A PHYSICAL

www.elsevier.nl/locate/sna

Improving yield, accuracy and complexity in surface tension self-assembled MOEMS

R.R.A. Syms[a,*], C. Gormley[b], S. Blackstone[b]

[a]*Optical and Semiconductor Devices Section, Department of Electrical and Electronic Engineering, Imperial College, Exhibition Road, London SW7 2BT, UK*

[b]*BCO Technologies (NI) Ltd., 5 Hannahstown Hill, Belfast BT17 OLT, UK*

Received 25 April 2000; accepted 31 October 2000

Abstract

An advanced process for self-assembly of three-dimensional micro-opto-mechanical systems (MOEMS) is demonstrated, based on deep reactive ion etching of bonded silicon-on-insulator material, sacrificial etching, and out-of plane rotation powered by the surface tension of thick photoresist pads. Improvements in structure definition and design are described, which have led to an increase in process yield to approximately 75% and in the best assembly accuracy to <0.1°. Optical mirrors oriented at 45 and 90° to the substrate are demonstrated by simultaneous and sequential self-assembly, respectively. Profile measurements of assembled structures show very high surface quality, and distortions of parts by surface tension forces are identified.

Keywords: MOEMS; Micro-optics; MEMS; Microsystems technology; Micro-mirror; Self-assembly

1. Introduction

Three-dimensional micro-opto-electro-mechanical systems (MOEMS) is a relatively new discipline, in which microfabrication and assembly are used to create small optical sub-systems that process quasi-free space beams travelling above the surface of a chip. Examples of components that have already been demonstrated include fixed components such as collimating lenses [1–5], Fabry–Perot etalons [6,7] and beamsplitters [8], and dynamically adjustable components such as moving mirror switches [9–15], scanners and bar code readers [16–19], display systems [20], corner cube reflectors [21], external cavity lasers [22] and focusing micro-stages [23]. Recent surveys of MOEMS can be found in [24,25].

MOEMS fabrication is generally based on multilayer polysilicon surface micro-machining [26–30], while assembly is based on out-of-plane rotation using microhinges [31–37]. A variety of methods have been used to power the rotation, including surface micro-machined microengines [38–40] and linear vibromotors [41,42]. Although these allow dynamic repositioning, they are complex and require large chip area. Attention is therefore now focused on more compact mechanisms.

A number of possibilities have been suggested for powering rotation, including magnetic deflection [43,44] and polymer shrinkage by thermal [45–48] and electrochemical [49–51] means. All are reversible, and thermal shrinkage in particular has allowed some impressive demonstrations. An alternative is offered by surface tension powered self-assembly, originally proposed by Imperial College in 1993 [52]. Because of the advantageous scaling of surface tension forces into the microstructure size domain, this method allows very compact geometries. However, it allows one-time operation, and so is most suited to structural assembly rather than actuation.

In surface tension self-assembly, small pads of a meltable material are used to link the edges of a fixed and a movable part, which are both initially coplanar. Before melting, the pads have a rectangular cross-section, and after melting, a semi-cylindrical section. By considering either the forces acting or the energy of the free liquid surface, it is possible to show the existence of a torque that tends to rotate the movable part out-of-plane [52,53]. Surface tension self-assembly has been demonstrated by us using small meltable pads of solder [53,54] and low melt temperature glass [55]. A MUMPS-type surface micromachining process based on small solder beads has also been developed elsewhere [56–

* Corresponding author. Tel.: +44-20-7594-6203; fax: +44-171-594-6308.
E-mail address: r.syms@ic.ac.uk (R.R.A. Syms).

0924-4247/00/$ – see front matter
PII: S0924-4247(00)00523-9

59]. However, in each case, there have been difficulties in achieving sufficient yield and alignment accuracy for the construction of realistic devices.

Recently, we demonstrated a considerably improved surface micromachining process based on mechanical parts formed from 4″ industry-standard bonded silicon-on-insulator (BSOI) wafers by conventional reactive ion etching (RIE), and meltable pads of thick photoresist, Hoechst AZ4562 [60–62]. The process was simple (involving just two masks, one dry etch step and one wet etch step), and used a novel simultaneously-assembled mechanical limiter to achieve an alignment accuracy of approximately 0.5 for 45° rotated structures. Although its yield was low, the process allowed the construction of a range of fixed 45° mirrors and electrostatic torsion mirror scanners.

In this paper, we describe further enhancements to the process obtained by deep reactive ion etching (DRIE) of the mechanical parts, introduce improved hinge designs, and demonstrate a sequential form of self-assembly that extends the technique of simultaneous assembly used for 45° mirrors to 90° rotated structures. The process is first described, and the influence of critical fabrication steps such as lithography and etching on uniformity, yield and assembly accuracy are discussed. Alignment errors below 0.1° are demonstrated for both 45 and 90° mirrors for the first time, and the surface flatness of assembled structures is shown to be extremely high (although it is shown that surface tension forces are strong enough to cause small structural distortions). These advances greatly enhance the prospects for self-assembled MOEMS.

2. Process and design improvements

Bonded silicon-on-insulator is rapidly becoming a material of choice for MEMS and MOEMS, because it allows the construction of thick, high quality suspended mechanical parts in single crystal material [63,64]. Our process is based BSOI material fabricated at BCO and consisting of 4″ Si(1 0 0) substrates carrying 5 μm thick bonded Si layers on 2 μm of thermal oxide (Fig. 1). In previous work, parts have been formed in the bonded layer by conventional RIE using a Cr hard mask [60–62]. Replacing this process with DRIE allows feature size control to be improved from 2 to 0.2 μm. This improvement in dimensional control increases the accuracy of the assembled structure, while the use of a stop-on-oxide etch increases uniformity and reduces the likelihood of failure caused by direct adhesion of the resist to the substrate.

Two lithography steps are involved. To define the parts, the wafers were patterned using the structural feature mask by UV lithography, using a Quintel Q4000-IR aligner to expose a 0.35 μm thick layer of Shipley S1400-17 photoresist spin coated at 5000 rpm for 40 s. Part sizes were typically of order 1 mm, with clearances between moving parts of 4 μm. The surface pattern was then transferred to the bonded layer by deep reactive ion etching in a Surface Technology Systems Single-Chamber Multiplex ICP Etcher, using the BCO/STS Advanced Silicon Etch (ASE^{TM}), a stop-on-oxide DRIE process [65–69].

The ASE^{TM} process uses alternating cycles of ICP etching and passivation at circa 25 mTorr pressure to etch silicon to depths >200 μm at high rates and with excellent sidewall verticality. In the etch step, sulphur hexafluoride is used to remove silicon by dissociating SF_6 into fluorine radicals. Although the etch process is isotropic, lateral erosion is prevented by a short polymer deposition step after each etch. This forms a layer of passivation (C_xF_y) on the surface of the feature by ionisation and dissociation of octafluorocylcobutane (C_4F_8). To re-initiate etching, fluorine radicals first etch the base of the passivation, and then the silicon itself. Although cyclic processing leads to sidewall scallops, these can be minimised by careful adjustment of the etch parameters. After etching, the resist mask was stripped.

To form the meltable pads, the etched wafers were spin-coated with Hoechst AZ4562 photoresist, pre-baked at 90°C, exposed to the hinge driver pad mask using the Quintel aligner, and developed in Hoechst AZ400 K developer (1:4 in DI water) for 6 min. The pads were formed in segmented blocks with dimensions of 250 μm × 40 μm. A pad thickness of 11.8 μm was used, obtained by spin coating at 1400 rpm for 40 s.

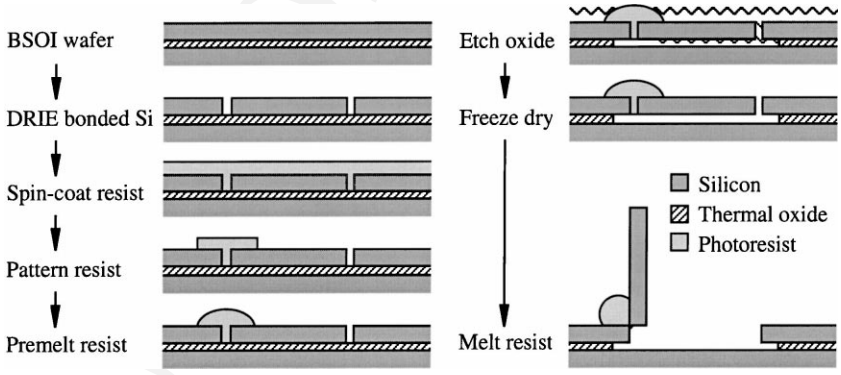

Fig. 1. Process flowchart for surface tension self assembly.

To free the mechanical parts, the buried oxide was then removed by wet etching for 10 h in 7:1 buffered hydrofluoric acid, which penetrated through 4 μm square holes on a 20 μm square pitch in the movable parts. The remaining wash water was then removed by freeze-drying. To assemble the structure into its three-dimensional configuration, the resist pads were remelted in a convection oven at 145°C. Finally, to improve reflectivity, the devices were sputter-coated with 500 Å of Al metal.

Previous demonstrations of resist-powered self-assembly have suffered from low yield, caused by (a) detachment of the movable parts, (b) stick-down, and (c) poorly-controlled rotation rates. Very significant improvements in process yield and assembly uniformity have been achieved by the following simple process changes.

Adhesion of the thick AZ4562 layer to the silicon parts was found to be substantially increased by cleaning the substrate in fuming nitric acid before spin coating, and by premelting the resist pads at 100°C for 30 min before sacrificial layer etching. However, despite this treatment, detachment of many of the movable parts occurred during the long HF etch. This problem was effectively eliminated by perforating the silicon lands on either side of the hinge using a series of 2 μm × 4 μm holes, as shown in Fig. 2, so that the solid resist pad effectively pinned the fixed and moving parts together during etching. Fig. 3 shows SEM views of the rear of a part after self-assembly, showing (a) the overall structure, and (b) a close-up of a single perforation though the moving part. The perforation is completely filled by resist, implying that the resist pins remain to reinforce the structure even after remelting and assembly.

Previous demonstrations of self-assembly have used freeze-drying [70] to remove rinse water after sacrificial etching without surface tension collapse [71]. The samples were simply placed in water in an Edwards Modulyo freeze-drier, which was connected to a vacuum line. Freezing occurred as the pressure reduced, but only after a short period of violent boiling, which caused many large movable parts to become detached. Degassing provided only limited improvement.

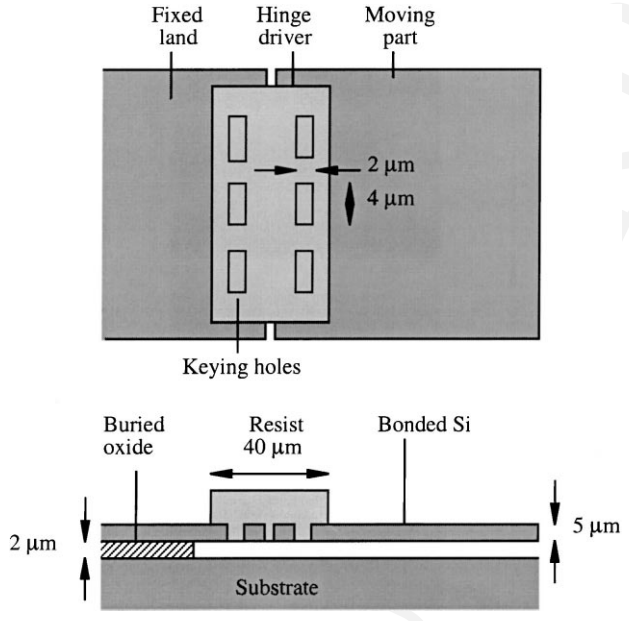

Fig. 2. Layout of improved hinge structure.

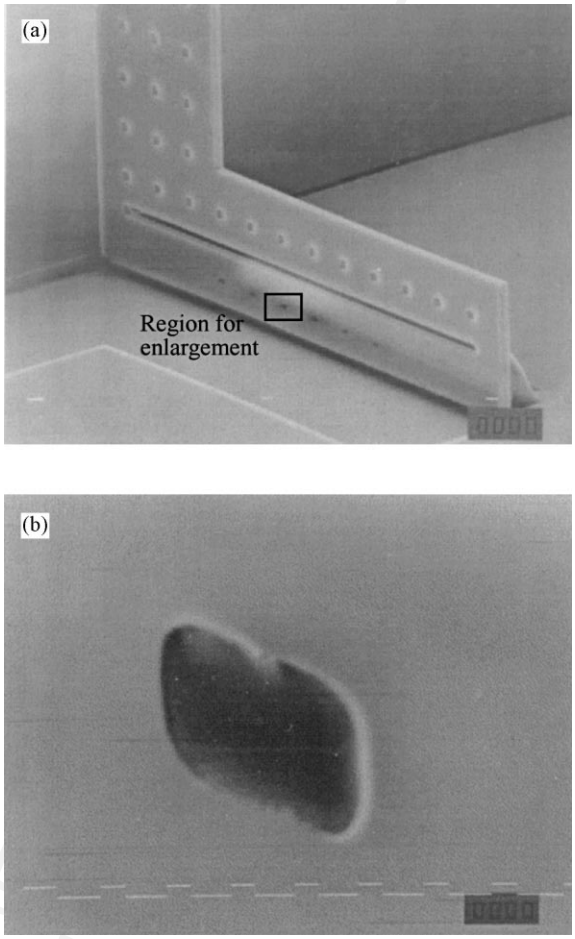

Fig. 3. SEM views of rear of 90° rotated part, showing (a) overall structure; (b) close up of hinge keying hole, showing complete infill by resist.

As the pressure reduced still further, the water finally froze and was removed by sublimation. However, more parts were found to be detached by the spontaneous cracking which always occurred during ice formation. In an attempt to improve yield, the water was replaced by a 25% solution of methanol in water, which formed a soft ice and froze without cracking. However, separate tests showed that most organic liquids (including cyclohexane, methanol, propan-1-ol, propan-2-ol, propylene carbonate, etc.) either dissolve the resist pads or weaken their adhesion. The following alternative procedure has therefore been developed. Samples are simply placed faced-down in open dishes containing ultrapure distilled water, frozen solid in a separate fridge, and only then placed in the freeze dryer. The pressure may then be lowered so that sublimation takes place without either gas evolution or cracking.

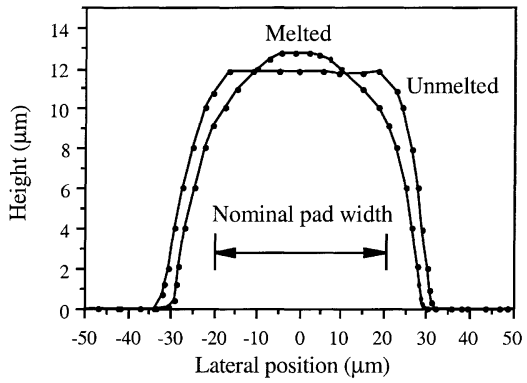

Fig. 4. Surface profiles measured for unmelted and melted photoresist hinge driver pads.

A final significant cause of low yield was also identified. After freeze drying, it was found that many of the remaining movable parts were collapsed down on to the substrate. This failure mode was traced to the formation and subsequent evaporation of condensate on the released parts, when warm air was admitted to the relatively cold freeze dryer during venting. This effect is significant for the suspended movable parts used here, because they are so large. It was eliminated simply by venting to dry N_2 while warming the substrates gently with a radiant heater. Taken together, these improvements have increased yield from around 5 to 75%.

Rotation rates may be controlled by improving the dimensional uniformity of the hinge driver pads. Fig. 4 shows typical pad profiles, measured before and after premelting, using a Dektak IIa surface profiler with a stylus tip radius of 25 μm. The profiles are unrealistic, because the pad heights are comparable with the tip radius, but an approximation to the initial rectangular and final parabolic profiles may be discerned.

More usefully, Fig. 5 shows measurements of the central height of 12 unmelted hinge driver pads. The pads belong to an array of three self-assembling mirrors, and are located on a mesa etched in the SOI layer. The resist height drops near the middle of each device, because of the draining effect of the perforations that are cut in the movable parts to allow later penetration of the undercut etch. Resist is also sucked into the etched trenches that separate all the parts. Pad uniformity is also reduced by proximity to the mesa edge. The former effect introduces a variation of ±0.05 μm in pad height (i.e. ±0.5%), while the latter increases the variation to ±0.1 μm (±1%). These measurements suggest that uniformity will be enhanced by ensuring that the etched silicon surface contains few open areas, so that the thick resist may accurately planarize the surface.

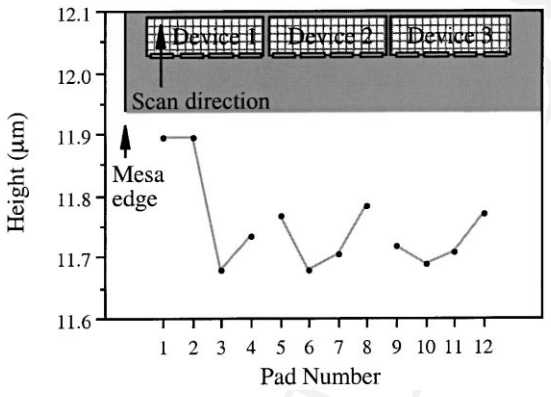

Fig. 5. Height of unmelted hinge driver pads as a function of position on the wafer.

3. 3D MOEMS components

Three-dimensional MOEMS components have previously been based on parts rotated 45° out-of-plane [60–62]. Rotation is powered by melting the resist pads, and the geometry of the assembly is fixed by a mechanical limiter. Fig. 6a shows the mechanism, which involves simultaneous rotation of two parts in opposite directions. Limiters on the parts engage to prevent further rotation when each has rotated through 45°. The accuracy of the mechanism is high, because it involves a long lever arm, and because the

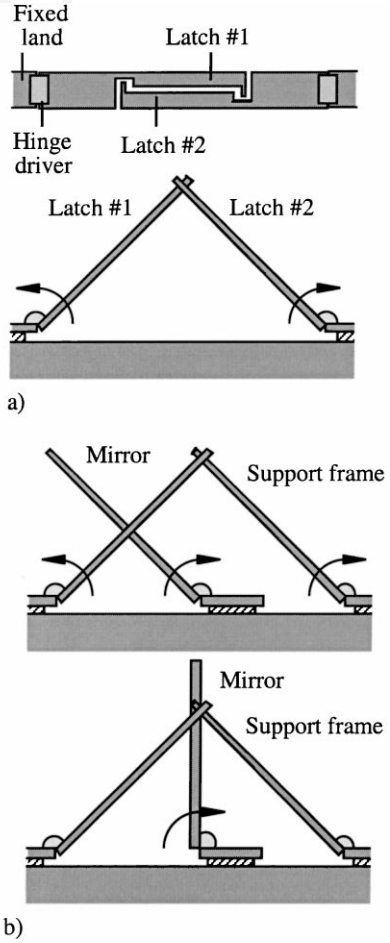

Fig. 6. Mechanical limiters for (a) simultaneously-assembled 45° mirrors, and (b) sequentially-assembled 90° mirrors.

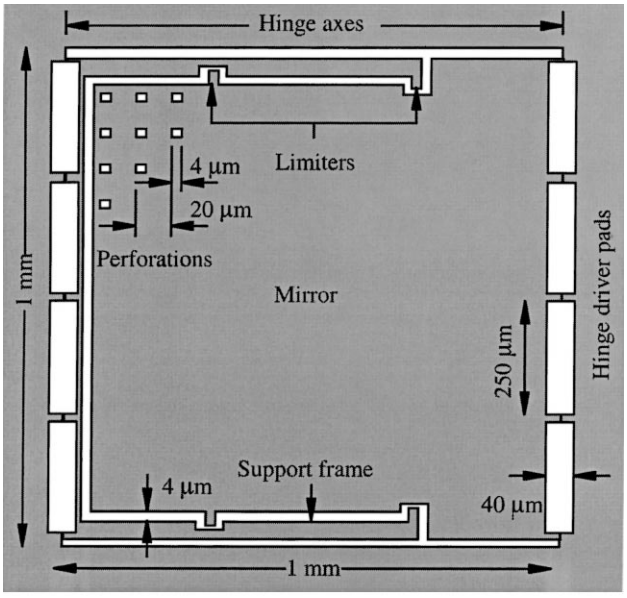

(a)

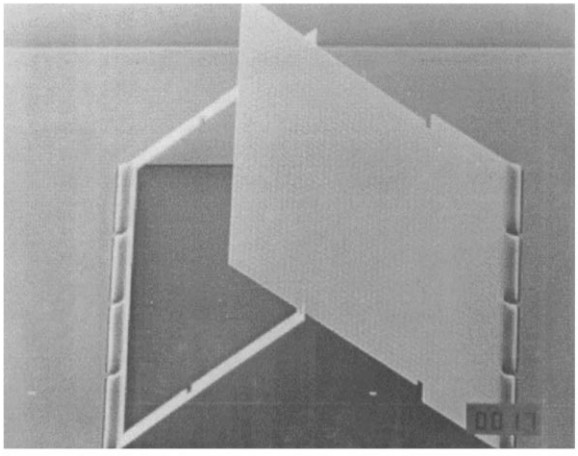

(b)

Fig. 7. (a) Schematic and (b) SEM view of simultaneously-assembled 45° mirror.

construction is determined almost exclusively by the geometric layout of the parts. Fig. 7a shows the CAD layout and Fig. 7b an SEM view of a 45° mirror based on this mechanism. The main difference from previous results is that the mirror span has been increased to almost 1 mm, and the support frame cut away as far as possible.

Remelting the resist, or overmelting to temperatures greater than that used for that used for the original assembly, does not cause the three-dimensional structure to collapse or the latch to release. However, greatly prolonged heating does cause degradation to the resist pads, which tend to creep back from their original lands and fragment into semispherical beads.

Despite the increased asymmetry in size and shape of the two halves of the structure, assembly has occurred with increased accuracy, suggesting that assembly dynamics are still dominated by the viscosity of the meltable pads rather

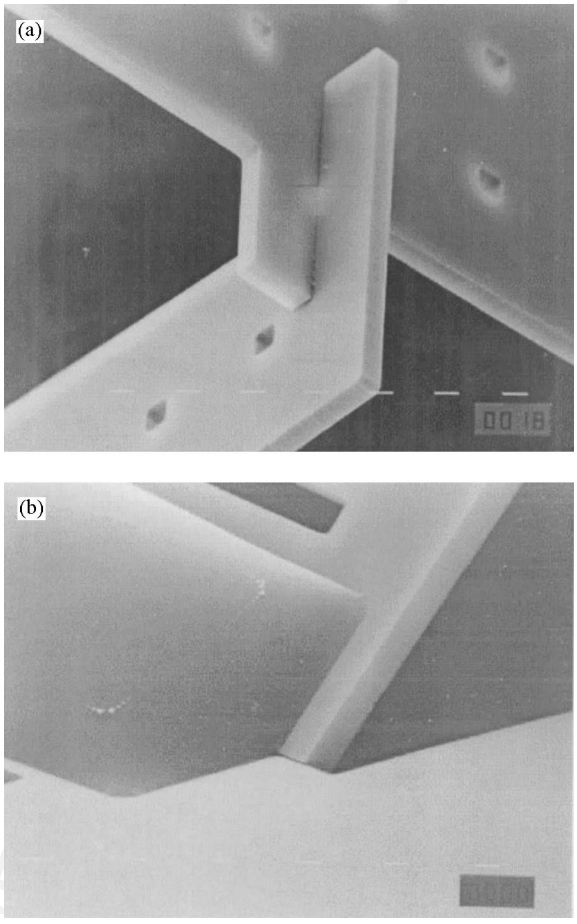

Fig. 8. Close-up SEM views of (a) limiter mechanism and (b) hinge driver of 45° mirror.

than by the weight of the parts. Fig. 8a and b show close-up SEM views of the engaged latch mechanism and hinge driver pad, respectively. At this magnification, there is no discernible gap between the parts at either point. Higher magnifications show typical misalignment between nominally engaged parts of ≈0.25 μm. These results illustrate the very high potential accuracy offered by the assembly method.

Angular measurements of assembled structures were performed by back reflection, using a HeNe laser and a goniometer calibrated in 2 arc min steps. Table 1 shows measurements obtained from 10 similar mirrors, which

Table 1
Angular measurements for a sample population of 10 self-assembled 45° mirrors

Mirror angle	No. of occurrences
44°54′	2
44°56′	2
44°58′	2
45°0′	1
45°2′	1
45°4′	2

clearly suggest that assembly accuracies of a few minutes may be routinely achieved, an approximate 10-fold improvement over previous results. This advance now makes the method appropriate for passively-assembled MOEMS.

The surface quality and flatness of assembled mirrors was assessed using a Zygo MetroPro^{TM} interferometric optical profilometer. Structures were simply mounted in a 45° vee-block, so that the relevant feature was then horizontal, and scanned in the normal way. Metrology was performed using 10 objective lens, scanned through a vertical distance of ±10 μm, with a zoom factor of 0.5.

Similar surface shapes were obtained from metallised and unmetallised samples, suggesting that metallisation stresses do not cause significant deformation, since all surfaces of the relatively open-framed structures receive coverage during sputter coating. However, some distortions of the structures were observed. For example, Fig. 9a shows a contour representation of the deformed shape of an uncoated 45° mirror support frame. The two support arms have a convex profile, and are slightly twisted. Fig. 9b shows a levelled profile scan along the line X–X′, which shows a maximum out-of-plane bow of approximately 1 mm.

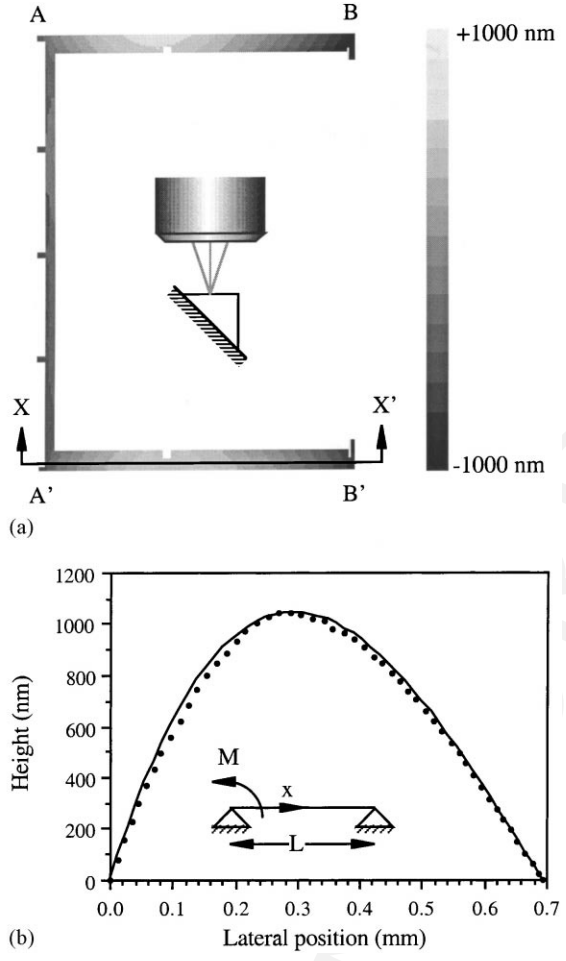

Fig. 9. (a) Contour representation of the surface flatness of a 45° mirror frame, and (b) surface profile measured along the line X–X′. Points are experimental data; solid lines are derived from simple beam bending theory.

This shape is consistent with the application of a moment about the axis A–A′ by the four hinge driver pads, and a constraint at the points B and B′ by the remainder of the structure. It provides the first evidence that surface tension torques may deform microstructures during assembly. However, since gravitational forces scale linearly with structural thickness, while resistance to bending is dependent on the cube of thickness, there is scope to reduce this distortion by a small increase in the thickness of the bonded layer.

Ignoring the twist, we may construct a one-dimensional model of each arm as a beam of approximately uniform second moment I and length L, that is subjected to a bending moment M at the left-hand end (caused by the hinge driver pads) and a restraint at the right-hand end (applied by the other element of the assembly, the mirror itself). The variation in vertical displacement y with position x along the beam may be obtained from simple bending theory as $y(x) = (M/EIL)\{L^2x/3 - Lx^2/2 + x^3/6\}$, where E is Young's modulus. This variation is shown superimposed on Fig. 9b, with the peak theoretical displacement matched to the experimental data. Excellent agreement in the deflected shape is obtained, given the simplicity of the model.

By assuming experimental dimensions for L and I, and assuming $E = 1.08 \times 10^{11}$ N/m^2 for Si, the surface tension torque acting on each arm may then be estimated as $M \approx 1.3 \times 10^{-9}$ Nm. This torque is effectively derived from two hinge driver pads per arm, and is in reasonable agreement with earlier estimates of the torque available using these pad dimensions [52].

Fig. 10a and b show contour and isometric representations of the other part of this structure, the 45° mirror itself. The surface is approximately flat near the hinge axis C–C′, convex near the centre, and symmetric about the horizontal centreline. Again, this shape is consistent with the existence of a torque along C–C′ and restraints at D and D′ provided by the mirror support. The mirror quality is extremely high, with a maximum height variation of approximately ±0.35 μm over the whole area (≈1 mm^2). This result corresponds to $\approx\lambda/2$ flatness for $\lambda = 1.5$ μm, suggesting promise for near infrared operation. The flatness is variable, with a worst-case radius of curvature (for bending parallel to the assembly axis) of 0.22 m.

Based on the improvements in assembly accuracy described above, it is now realistic to consider more complex assembly operations. For example, time-sequential self-assembly allows the demonstration of 90° rotated structures, as shown in Fig. 6b. Here, simultaneous assembly using the limiter mechanism of Fig. 6a is first used to construct a ''stop'' in mid air above the substrate, which then prevents further rotation of an additional mirror component after it has rotated through 90°. Assembly is sequential, because the mirror must rotate through a larger angle than the parts used to form the support frame. However, the timings are not

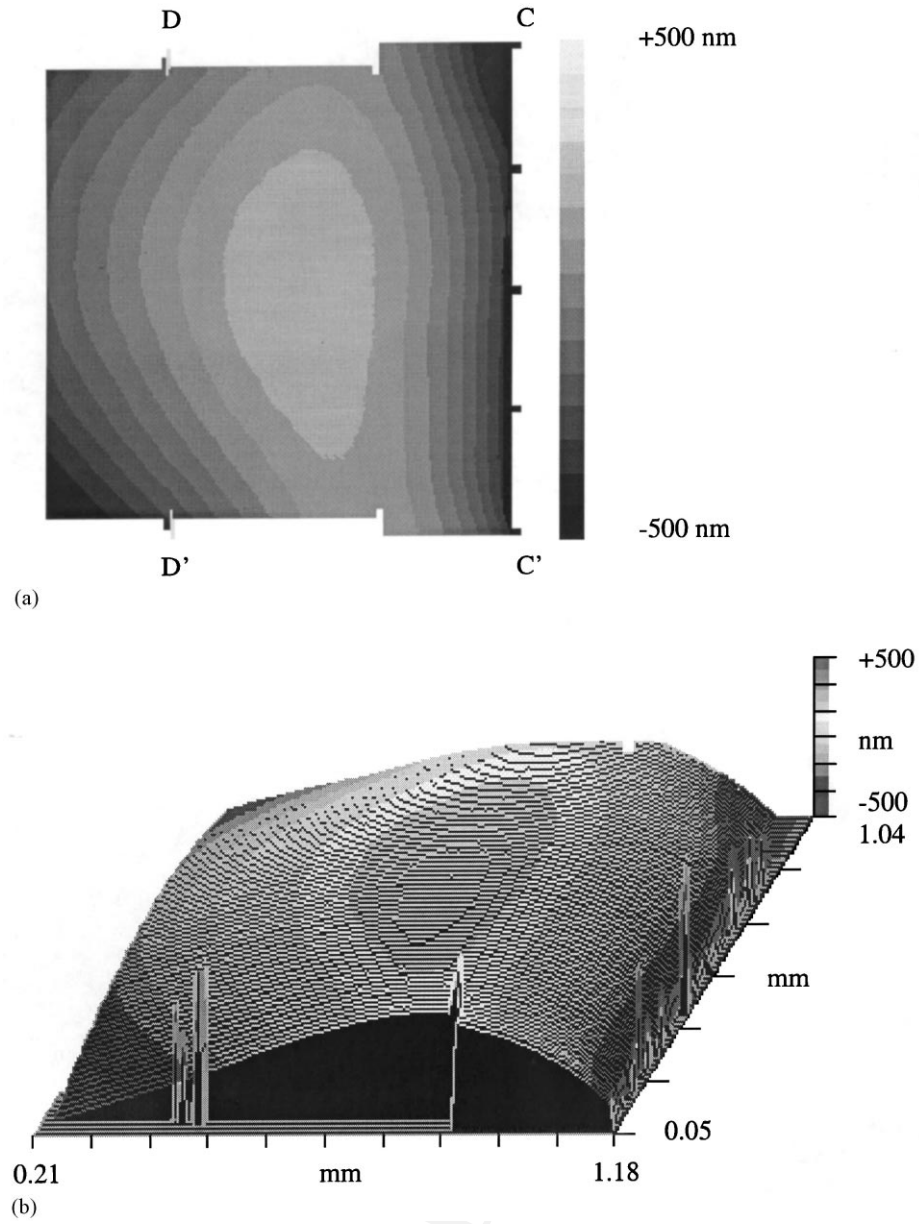

Fig. 10. (a) Contour and (b) isometric representations of the surface flatness of a 45° mirror.

crucial; the only requirement is that the mid-air stop be completed before the mirror reaches it.

Fig. 11a shows the CAD layout of a 90° mirror constructed by this technique. The frame is constructed from two separate limiters, placed on either side of the mirror and ganged together by the link bars 1 and 2 to minimise the number of separate moving parts. Link bar 2 provides the mid-air 'stop'. Fig. 11b shows an SEM view of the final structure, which has clearly assembled as predicted. Fig. 12a shows a close-up SEM view of the stop mechanism, showing that the three moving parts have actually engaged to submicron accuracy. Fig. 12b shows a close-up SEM view of the base of the 90° mirror. The periodic patterns on the mechanical parts in this view are the scallops referred to in Section 2. There is no discernible gap between the mirror and its baseplate, but the mirror has descended vertically by ≈0.7 μm.

Some photoresist is visible on the original vertical edges of both the fixed and movable part in Fig. 12b, suggesting good adhesion to the sidewalls of trenches etched into the bonded Si layer. Interestingly, the resist surface profile in this region is concave. Since the corresponding free surface on the hinge driver pads is convex, there must have been a difference in the Laplace pressure between the two regions during rotation. Simple theory would suggest that molten resist would be transferred between the two regions until the pressures equalised. Because this clearly has not occurred, the apex of the hinge gap must have closed hermetically. In future designs, it may be advantageous to include openings along the hinge to allow the passage of resist, because a

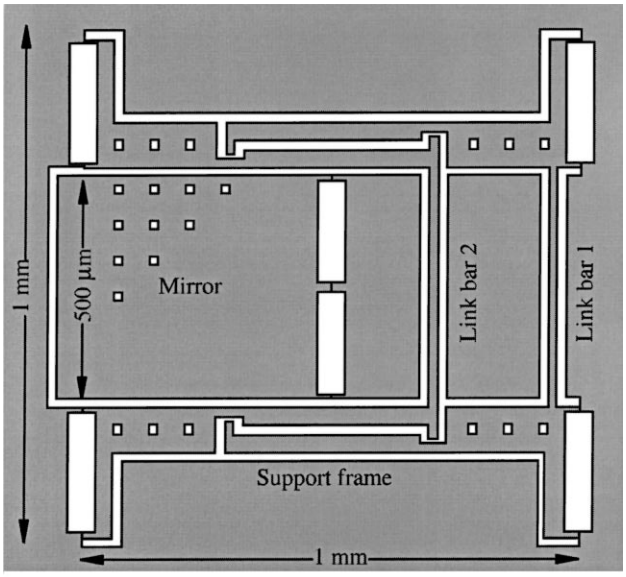

(a)

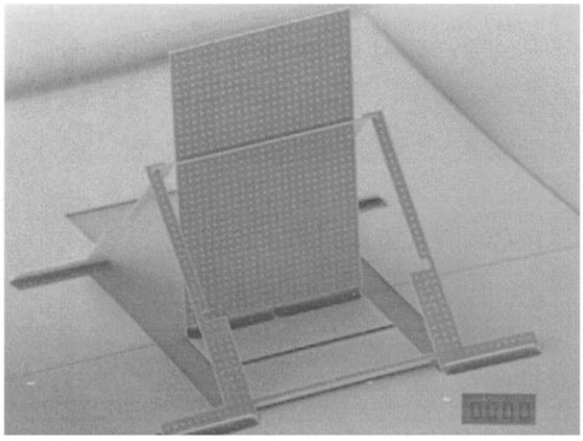

(b)

Fig. 11. (a) Schematic and (b) SEM view of sequentially-assembled 90° mirror.

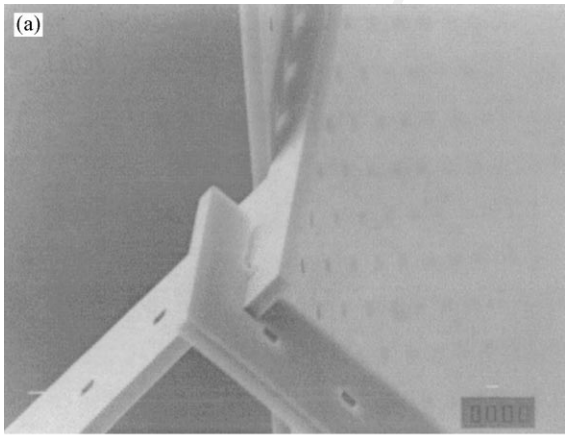

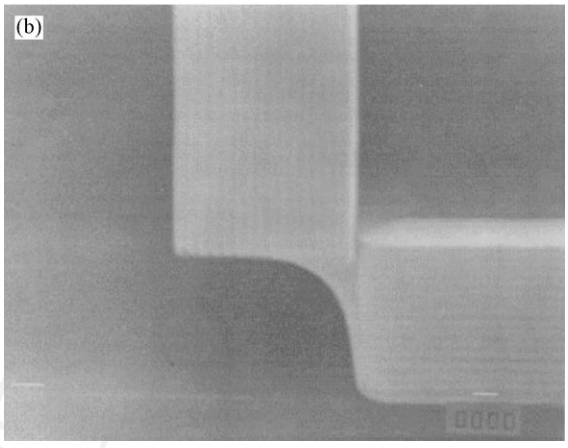

Fig. 12. Close-up SEM views of (a) limiter mechanism and (b) hinge driver of 90° mirror.

negative Laplace pressure below the hinge must lead to a large counter torque acting to prevent rotation.

Final assembly of 90° mirrors took considerably longer than 45° mirrors, in some cases up to 1 h at 155°C, possibly because of the counter-torque described above. However, correct assembly generally occurred eventually, and the supporting frame did not appear to be disturbed by the excessive melting. Some dependence of the assembly time on part size was also observed; mirrors with final heights of 500 μm assembled considerably more quickly than those with final heights of 1 mm. It may, therefore, be that parts of these dimensions are approaching the practical limit for assembly by a surface micromachining process.

Surface profiles were again obtained of parts of the assembled structure, this time with the aim of determining whether the considerable additional thermal treatment described above would lead to excessive distortion of the relatively flimsy mirror support frame. Fig. 13a shows a contour representation of the surface of the front member of the frame. The surface is clearly convex again, confirming that the surface tension torque acting at the hinge has again bent this part out of plane after the limiters have engaged. Interestingly, there are signs of stress concentrations around the hinge driver pads. However, Fig. 13b shows a profile measured along the line X–X′. The maximum bow is roughly half the value shown in Fig. 9b, which is consistent with a bending moment of approximately half that found for the 45° mirror frame. This reduced moment is in turn consistent with the reduced number (two) of hinge driver pads used to assemble the 90° mirror frame. The overall conclusion is that the additional heating needed to assemble the 90° mirror has not significantly increased the structural deformation.

Once again, it should be emphasised that surface tension self-assembly is a mass assembly process and that operations as complex as sequential assembly may be carried out accurately in parallel. Fig. 14 shows a SEM view of a group of four assembled 90° structures. The angular alignment of the two structures at the front were measured by back reflection as 89°56′ (LH) and 90° (RH), respectively.

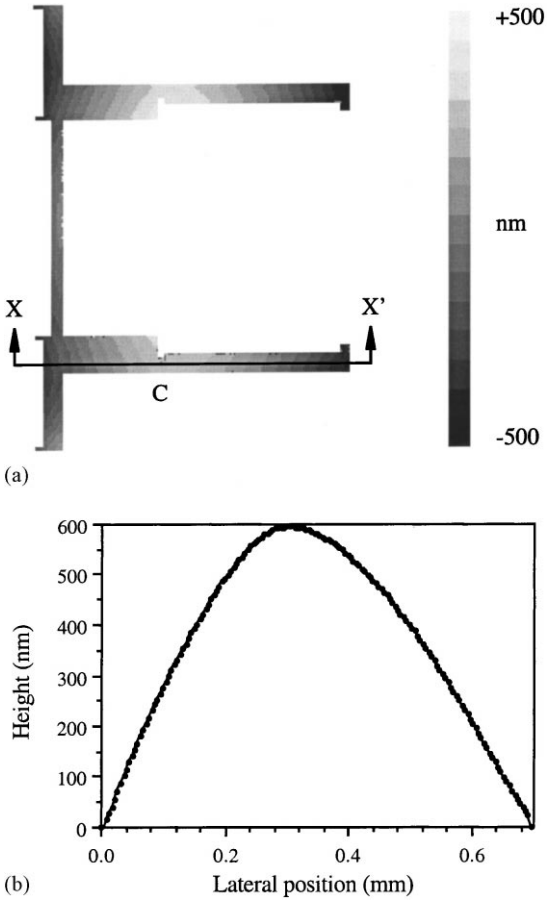

Fig. 13. (a) Contour representation of the surface of the front member of a 90° mirror frame, and (b) surface profile measured along the line X–X′.

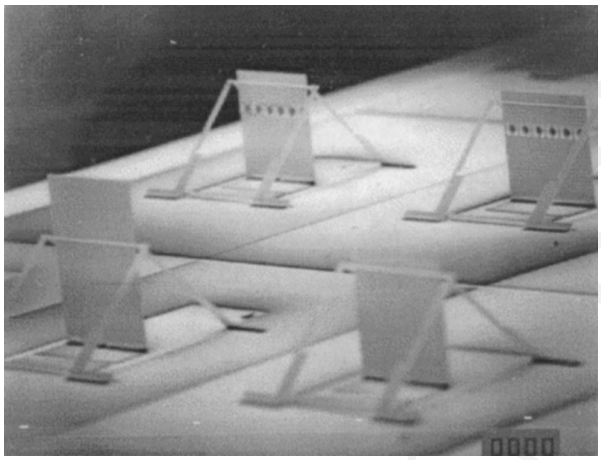

Fig. 14. SEM view of group of 90° mirrors assembled in parallel.

4. Conclusions

We have shown that the use of deep reactive ion etching for structural definition, together with improved hinge and mechanism designs, can allow a substantial increase in the yield, accuracy and complexity of surface tension self-assembled silicon based 3D MOEMS components.

Process yield has been improved to a realistic level (75%) and angular alignment errors have been reduced to a few minutes of arc. The surface quality of nominally planar mirrors has been shown to be extremely high, although some small structural distortions caused by the surface tension forces used to power the assembly operation have been identified. The technique of mechanical limiting by simultaneous self-assembly has been extended to allow structures to be assembled in a definite sequence.

Acknowledgements

The Author is very grateful to Matt Solomon for assistance with optical surface profiling. The financial support of the EPSRC through Grant GR/L90286 is also gratefully acknowledged.

References

[1] L.Y. Lin, S.S. Lee, K.S.J. Pister, M.C. Wu, Three-dimensional micro-Fresnel optical elements fabricated by micromachining techniques, Elect. Lett. 30 (1994) 448–449.
[2] L.Y. Lin, S.S. Lee, K.S.J. Pister, M.C. Wu, Micromachined micro-optical bench for optoelectronic packaging, in: Proceedings of the 7th Annual Meet, IEEE Lasers and Electro-Optics Society, Boston, MA, USA, 31 October–3 November 1994, pp. 219–220.
[3] S.S. Lee, L.Y. Lin, K.S.J. Pister, M.C. Wu, H.C. Lee, P. Grodzinski, Passively aligned hybrid integration of 8 × 1 micromachined micro-Fresnel lens arrays and 8 × 1 vertical-cavity surface-emitting laser arrays for free-space optical interconnect, IEEE Photon. Technol. Lett. 7 (1995) 1031–1033.
[4] M.C. Wu, L.-Y. Lin, S.-S. Lee, K.S.J. Pister, Micromachined free-space integrated micro-optics, Sens. Actuators A 50 (1995) 127–134.
[5] C.R. King, L.Y. Lin, M.C. Wu, Out-of-plane refractive microlens fabricated by surface micromachining, IEEE Photon. Technol. Lett. 8 (1996) 1349–1351.
[6] J.L. Shen, L.Y. Lin, S.S. Lee, M.C. Wu, M. Sergent, Surface-micromachined tunable three-dimensional solid Fabry-Perot etalons with dielectric coatings, Elect. Lett. 31 (1995) 2172–2173.
[7] L.Y. Lin, J.L. Shen, M.C. Wu, A.M. Sergent, Tunable three-dimensional solid Fabry–Perot etalons fabricated by surface micromachining, IEEE Photon. Technol. Lett. 8 (1996) 101–103.
[8] C. Pu, Z. Zhu, Y.-H. Lo, Surface micromachined integrated optic polarization beam splitter, IEEE Photon. Technol. Lett. 10 (1998) 988–990.
[9] S.S. Lee, L.Y. Lin, M.C. Wu, Surface micromachined free-space fiber optic switches, Elect. Lett. 31 (1995) 1481–1482.
[10] L.Y. Lin, E.L. Goldstein, J.M. Simmona, R.W. Tkach, Free-space micromachined optical switches with submillisecond switching time for large-scale optical crossconnects, IEEE Photon. Technol. Lett. 10 (1998) 525–527.
[11] L.Y. Lin, E.L. Goldstein, J.M. Simmons, R.W. Tkach, High-density micromachined polygon optical crossconnects exploiting network connection-symmetry, IEEE Photon. Technol. Lett. 10 (1998) 1425–1427.
[12] S.S. Lee, L.S. Huang, C.-J. Kim, M.C. Wu, Free-space fiber-optic switches based on MEMS vertical torsion mirrors, J. Lightwave Technol. LT-17 (1999) 7–13.

[13] L.Y. Lin, E.L. Goldstein, Lightwave micromachines for optical crossconnects, in: Proceedings of the 25th European Conference on Optical Communication (ECOC), Vol. I, Nice, France, 26–30 September 1999, pp. 114–117.
[14] L.Y. Lin, E.L. Goldstein, L.M. Lunardi, Connection-verification in optical-MEMS crossconnects via mirror-dither, in: Proceedings of the 25th European Conference on Optical Communication (ECOC), Vol. I, Nice, France, 26–30 September 1999, pp. 120–121.
[15] E.L. Goldstein, L.Y. Lin, R.W. Tkach, Optical-MEMS-based tail-end switching for restoration of line-rate services, in: Proceedings of the 25th European Conference on Optical Communication (ECOC), Vol. I, Nice, France, 26–30 September 1999, pp. 62–63.
[16] M.-H. Kiang, O. Solgaard, R.S. Muller, K.Y. Lau, Micromachined polysilicon microscanners for barcode readers, IEEE Photon. Technol. Lett. 8 (1996) 95–97.
[17] M.-H. Kiang, O. Solgaard, K.Y. Lau, Electrostatic combdrive-actuated micromirrors for laser-beam scanning and positioning, J. Micromech. Syst. 7 (1998) 27–37.
[18] J.R. Reid, V.M. Bright, J.H. Comtois, Arrays of thermal micro-actuators coupled to micro-optical components, Proc. SPIE 2865 (1996) 74–82.
[19] J.T. Butler, V.M. Bright, J.R. Reid, Scanning and rotating micro-mirrors using thermal actuators, Proc. SPIE 3131 (1997) 134–144.
[20] P.M. Hagelin, O. Solgaard, Optical raster-scanning displays based on surface micromachined polysilicon mirrors, IEEE J. Selected Topics Quantum Electron. 5 (1999) 67–74.
[21] D.S. Gunawan, L.Y. Lin, K.S.J. Pister, Micromachined corner cube reflectors as a communications link, Sens. Actuators A 46/47 (1995) 580–583.
[22] M.-H. Kiang, O. Solgaard, R.S. Müller, K.Y. Lau, Silicon micro-machined micromirrors with integrated high-precision actuators for external cavity semiconductor lasers, IEEE Photon. Technol. Lett. 8 (1996) 95–97.
[23] L.Y. Lin, J.L. Shen, S.S. Lee, M.C. Wu, Surface micromachined micro-XYZ stages for free-space micro-optical bench, IEEE Photon. Technol. Lett. 9 (1997) 345–347.
[24] M.C. Wu, Micromachining for optical and optoelectronic systems, Proc. IEEE 85 (1997) 1833–1856.
[25] R.S. Muller, Y.K. Lau, Surface micromachined micro-optical elements and systems, Proc. IEEE 86 (1998) 1705–1720.
[26] M. Mehregany, K.J. Gabriel, W.S.N. Trimmer, Integrated fabrication of polysilicon mechanisms, IEEE Trans. Electron Devices 35 (1988) 719–723.
[27] L.S. Fan, Y.-C. Tai, R.S. Muller, Integrated movable micromechanical structures for sensors and actuators, IEEE Trans. Electron Devices 35 (1988) 724–730.
[28] K.W. Markus, D.A. Koester, A. Cowen, R. Mahadevan, V.R. Dhuler, D. Robertson, L. Smith, MEMS infrastructure: the multi-user MEMS processes (MUMPS), Proc. SPIE 2639 (1995) 54–63.
[29] M.S. Rogers, J.J. Sniegowski, S.L. Miller, C.C. Barron, P.J. McWhorter, Advanced micromechanisms in a multi-level polysilicon technology, Proc. SPIE 3224 (1997) 120–130.
[30] J.M. Bustillo, R.T. Howe, R.S. Muller, Surface micromachining for microelectro-mechanical systems, Proc. IEEE 86 (1998) 1552–1573.
[31] K. Suzuki, I. Shimoyama, H. Miura, Y. Ezura, Creation of an insect-based microrobot with an external skeleton and elastic joints, in: Proceedings of the Micro Electro Mechanical Systems'92, Travemunde, Germany, 4–7 February 1992, pp. 190–195.
[32] K. Suzuki, I. Shimoyama, H. Miura, Insect model based microrobot with elastic hinges, IEEE J. Microelectromech. Syst. 3 (1994) 4–9.
[33] M.G. Allen, M. Scheidl, R.L. Smith, Design and fabrication of movable silicon plates suspended by flexible supports, in: Proceedings of the IEEE Microelectromechanical Syst. Workshop, February 1989, pp. 76–81.
[34] M.G. Allen, M. Scheidl, R.L. Smith, Movable micromachined silicon plates with integrated position sensing, Sens. Actuators A 21–23 (1990) 211–214.
[35] K.S. Pister, M.W. Judy, S.R. Burgett, R.S. Fearing, Microfabricated hinges, Sens. Actuators A 33 (1992) 249–256.
[36] R. Yeh, E.J.J. Kruglick, K.S.J. Pister, Surface-micromachined components for articulated microrobots, J. Microelectromech. Syst. 5 (1996) 10–17.
[37] A. Friedberger, R.S. Müller, Improved surface-micromachined hinges for fold-out structures, J. Microelectromech. Syst. 7 (1998) 315–319.
[38] E.J. Garcia, J.J. Sniegowski, Surface micromachined microengine, Sens. Actuators A 48 (1995) 203–214.
[39] J.J. Sniegowski, E.J. Garcia, Microfabricated actuators and their application to optics, Proc. SPIE 2383 (1995) 46–64.
[40] E.J. Garcia, Micro-flex mirror and instability actuation technique, in: Proceedings of the 11th International Workshop on MicroElectro Mechanical Systems, Heidelberg, 25–29 January 1998, pp. 470–475.
[41] N.J. Daneman, N.C. Tien, O. Solgaard, A.P. Pisano, K.Y. Lau, R.S. Muller, Linear vibromotor for positioning optical components, J. Microelectromech. Syst. 5 (1996) 159–165.
[42] N.C. Tien, O. Solgaard, M.H. Kiang, M. Daneman, K.Y. Lau, R.S. Muller, Surface micromachined mirrors for laser-beam positioning, Sens. Actuators A 52 (1996) 76–80.
[43] I. Shimoyama, O. Kano, H. Miura, 3D microstructures folded by Lorentz force, in: Proceedings of the 11th International Workshop on MicroElectroMechanical Systems, Heidelberg, 25–29 January 1998, pp. 24–28.
[44] Y.W. Yi, C. Liu, Magnetic actuation of hinged microstructures, J. Microelectromech. Syst. 8 (1999) 10–17.
[45] T. Ebefors, E. Kälvesten, C. Vieider, G. Stemme, New robust small radius joints based on thermal shrinkage of polyimide in V-grooves, in: Proceedings of the Tech. Dig. 9th International Conference on Solid-State Sensors & Actuators (Transducers'97), Chicago, USA, 16–19 June 1997, pp. 675–678.
[46] T. Ebefors, E. Kälvesten, G. Stemme, New small radius joints based on thermal shrinkage of polyimide in V-grooves for robust self-assembly 3D microstructures, J. Micromech. Microeng. 8 (1988) 188–194.
[47] T. Ebefors, E. Kälvesten, G. Stemme, Dynamic actuation of polyimide V-groove joints by electrical heating, Sens. Actuators A 67 (1998) 199–204.
[48] T. Ebefors, E. Kälvesten, G. Stemme, Three-dimensional silicon triple-hot-wire anemometer based on polyimide joints, in: Proceedings of the 11th International Workshop on MicroElectroMechanical Systems, Heidelberg, 25–29 January 1998, pp. 93–98.
[49] E. Smela, O. Inganäs, I. Lundström, Self-opening and closing boxes and other micromachined folding structures, in: Proceedings of the 8th International Conference on Solid-State Sensors and Actuators, Stockholm, 25–29 June 1995, pp. 350–351.
[50] E. Smela, O. Inganäs, I. Lundström, Controlled folding of micrometer-size structures, Science 268 (1995) 1735–1738.
[51] E. Smela, M. Kallenbach, J. Holdenried, Electrochemically driven polypyrrole plates for moving and positioning bulk micromachined silicon plates, IEEE/ASME J. Microelectromech. Syst. 8 (1999) 373–383.
[52] R.R.A. Syms, E.M. Yeatman, Self-assembly of fully three-dimensional microstructures using rotation by surface tension forces, Elect. Lett. 29 (1993) 662–664.
[53] R.R.A. Syms, Equilibrium of hinged and hingeless structures rotated using surface tension forces, J. Microelectromech. Syst. 4 (1995) 177–184.
[54] P.W. Green, R.R.A. Syms, E.M. Yeatman, Demonstration of three-dimensional microstructure self-assembly, J. Microelectromech. Syst. 4 (1995) 170–176.
[55] R.R.A. Syms, Rotational self-assembly of complex microstructures by the surface tension of glass, Sens. Actuators A 65 (1998) 238–243.
[56] K.F. Harsh, R.S. Irwin, Y.C. Lee, Solder self-assembly for MEMS, in: Proceedings of the 4th International Instrumentation Symposium, Reno, Nevada, 3–7 May 1998, pp. 256–261.

[57] K. Harsh, Y.C. Lee, Modelling for solder self-assembled MEMS, in: Proceedings of the SPIE 3289, San Jose, CA, 24–30 January 1998, pp. 177–184.
[58] K.F. Harsh, V.M. Bright, Y.C. Lee, Solder self-assembly for three-dimensional microelectromechanical systems, Sens. Actuators A 77 (1999) 237–244.
[59] P.E. Kladitis, V.M. Bright, Prototype microrobots for micro-positioning and micro-unmanned vehicles, Sens. Actuators 80 (2000) 132–137.
[60] R.R.A. Syms, Surface tension powered self-assembly of 3-D micro-optomechanical structures, IEEE/ASME J. Microelectromech. Syst. 8 (1999) 448–455.
[61] R.R.A. Syms, Operation of a surface-tension self-assembled 3-D micro-optomechanical torsion mirror scanner, Elect. Lett. 35 (1999) 1157–1158.
[62] R.R.A. Syms, S. Blackstone, 3-D self-assembly of optomechanical structures using bonded SOI, in: Proceedings of the 1999 Annual Meeting of the Electrochemical Society, Honolulu, Hawaii, 17–22 October 1999, paper 1026.
[63] A. Benitez, J. Esteve, J. Bausells, Bulk silicon microelectromechanical devices fabricated from commercial bonded and etched-back silicon-on-insulator substrates, Sens. Actuators A 50 (1995) 99–103.
[64] E.H. Klaassen, K. Petersen, J.M. Noworolski, J. Logan, N.I. Maluf, J. Brown, C. Storment, W. McCulley, T.A. Kovacs, Silicon fusion bonding and deep reactive ion etching: a new technology for microstructures, Sens. Actuators A 52 (1996) 132–139.
[65] F. Laermer, A. Schilp, Method of anisotropically etching silicon, US Patent 5,501,893 (1996).
[66] J.K. Bhardwaj, H. Ashraf, Advanced silicon etching using high density plasmas, Proc. SPIE 2639 (1995) 224–233.
[67] M.F. McNie, D.O. King, M.C.L. Ward, S. Blackstone, C. Quinn, J. Burdess, Deep reactive ion etching of SOI for silicon micromachined structures, Proc. Dig., International SOI Conference, Yosemite, October 1997, pp. 60–61.
[68] A.M. Hynes, H. Ashraf, J.K. Bhardwaj, J. Hopkins, I. Johnston, J.N. Shepherd, Recent advances in silicon etching for MEMS using the ASE^{TM} process, Sens. Actuators 74 (1999) 13–17.
[69] C. Gormley, K. Yallup, W.A. Nevin, J. Bhardwaj, H. Ashraf, P. Hugget, S. Blackstone, State of the art deep silicon anisotropic etching on SOI bonded substrates for dielectric isolation and MEMS applications, in: Proceedings of the 5th International Symposium on Semiconductor Wafer Bonding, Fall Meeting of the Electrochemical Society, Hawaii, USA, 17–22 October 1999.
[70] H. Guckel, D.W. Burns, Fabrication of micromachined devices from polysilicon films with smooth surfaces, Sens. Actuators 20 (1989) 117–122.
[71] C.H. Mastrangelo, C.H. Hsu, Mechanical stability and adhesion of microstructures under capillary forces. Parts I & II, J. Microelectromech. Syst. 2, 33–43 (Part I) & 44–55 (Part II) (1993).